Light-Induced Metastable Magnetic Texture Uncovered by *in situ* Lorentz Microscopy

Tim Eggebrecht,[1] Marcel Möller,[2] J. Gregor Gatzmann,[2] Nara Rubiano da Silva,[2] Armin Feist,[2] Ulrike Martens,[3] Henning Ulrichs,[1] Markus Münzenberg,[3] Claus Ropers,[2] and Sascha Schäfer[2,*]

[1]*I. Physical Institute, Georg-August-University, 37077 Göttingen, Germany*

[2]*IV. Physical Institute, Georg-August-University, 37077 Göttingen, Germany*

[3]*Institute of Physics, Ernst-Moritz-Arndt-University, 17489 Greifswald, Germany*

(Received 23 August 2016; published 1 March 2017)

Magnetic topological defects, such as vortices and Skyrmions, can be stabilized as equilibrium structures in nanoscale geometries and by tailored intrinsic magnetic interactions. Here, employing rapid quench conditions, we report the observation of a light-induced metastable magnetic texture, which consists of a dense nanoscale network of vortices and antivortices. Our results demonstrate the emergence of ordering mechanisms in quenched optically driven systems, which may give a general access to novel magnetic structures on nanometer length scales.

DOI: 10.1103/PhysRevLett.118.097203

Topologically protected magnetic defects cannot be continuously transformed into a defect-free state and therefore may be viewed as quasiparticles, largely robust against thermal perturbation [1]. Depending on the magnetic anisotropy of the structure, magnetic defects of different topology, such as vortices and Skyrmions, may exist, often stabilized in tailored nanostructures [2–6] or by intrinsic interactions [7,8]. For the latter case, as a prominent example, the chiral Dzyaloshinskii-Moriya interaction induces ordered Skyrmion lattices in helimagnetic materials, such as MnSi [9], $Fe_{1-x}Co_xSi$ [10], or in single-atomic iron layers on an iridium surface [11].

As expected for robust quasiparticles, magnetic defects can be manipulated by external perturbations, including (spin-polarized) currents [12–14], magnetic fields [15,16], thermal gradients [17,18], and optical excitations [19], but their temporal evolution remains to be constrained by topological invariants. For example, for vortices stabilized in magnetic nanodiscs, the reversal of the vortex core polarization upon radiofrequency excitation was observed to occur only over a sequence of vortex-antivortex generation and annihilation events, instead of the topologically forbidden direct flip of the core polarization [15,20–22].

Despite their intrinsic stability, topological defects can be created or destroyed at structural inhomogeneities, including particle boundaries [16] or channel constrictions [14]. More fundamentally, within a homogeneous film, topological defects may be formed in pairs of opposite topological character, such as vortices and antivortices, a process reminiscent of particle-antiparticle creation. Topological defect pair generation is particularly effective when crossing a second-order phase transition at fast quench rates, and was described to follow a universal behavior captured within the framework of the Kibble-Zurek mechanism (KZM) [23–25]. For nonmagnetic degrees of freedom, quench-induced defect pair generation was experimentally demonstrated in several solid-state systems, including nematic liquid crystals [26], two-dimensional layers of colloidal particles [27], ferroelectric materials [25,28], and in superfluidic ^{3}He [29,30], as well as in confined atomic neutral and ionized gases [31]. In contrast, in magnetic systems, KZM-like defect pair generation has remained elusive, and is expected to be observed only at large quench rates.

In this work, we demonstrate the formation of a metastable magnetic vortex-antivortex texture in a thin ferromagnetic iron layer after quenching from the paramagnetic state on picosecond time scales. Femtosecond optical excitation with a single laser pulse demagnetizes a micrometer-sized region of the iron film, and subsequent thermal quenching due to the substrate results in a dense nanoscale network of localized magnetic vortices and antivortices. Spatial correlations within the network structure are mapped *in situ* by Lorentz microscopy, exhibiting fluidlike pair-correlation functions.

In our experiments, bilayers composed of iron and silicon-nitride were prepared by depositing polycrystalline iron thin films (10 nm thickness, about 25 nm grain size) onto silicon nitride membranes (20 nm thickness, 28 μm $\times$ 17 μm membrane area) using electron beam evaporation in an ultrahigh vacuum environment. To map the optically induced magnetization changes in the bilayer system, we perform Lorentz microscopy in a transmission electron microscope, which was modified to allow for *in situ* femtosecond laser excitation. Out-of-focus conditions are utilized to acquire images with a contrast sensitive to the transverse sample magnetization [32]. High throughput imaging allows us to microscopically investigate irreversible magnetization changes and to acquire statistical properties of the optically induced changes. Magnetization changes are initiated by single ultrashort laser pulses (800 nm center wavelength, 150 fs pulse duration, 45 μm focal spot size), and the magnetic structure is imaged after each single laser pulse [cf. Fig. 1(a)]. Laser excitation at high pulse fluences results in an ultrafast heating of the iron film above its Curie temperature, followed by a rapid temperature quench due to the adjacent silicon nitride

 © 2017 American Physical Society

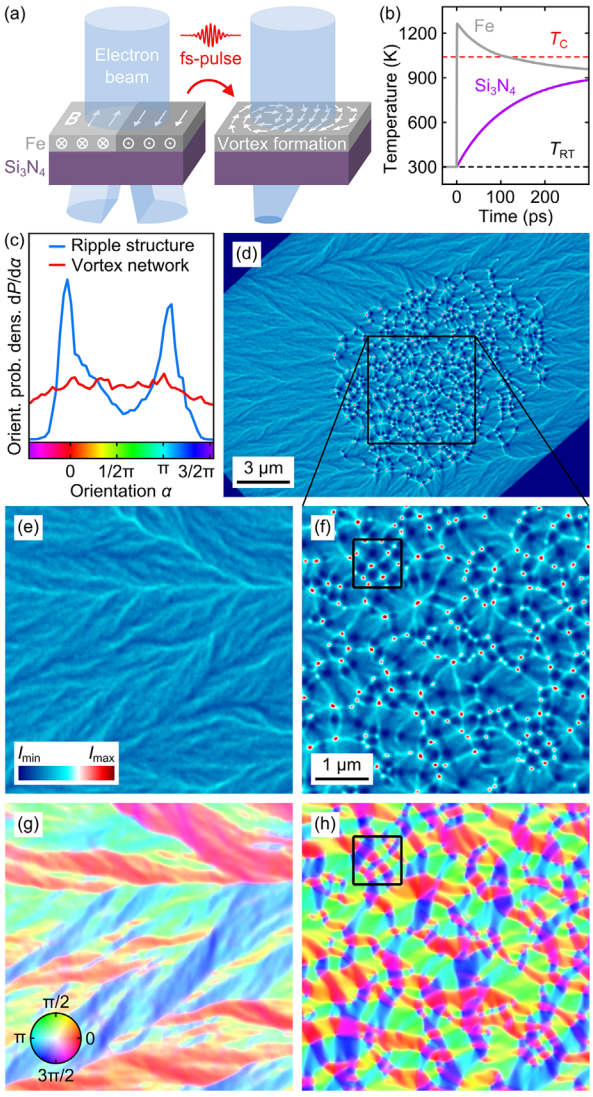

FIG. 1. Optically induced magnetic vortex-antivortex network. (a) The in-plane magnetization of an iron thin film is imaged by Lorentz microscopy employing *in situ* optical excitation. (b) Simulated temperature transient after optical excitation in the iron thin film and the silicon nitride substrate ($T_C = 1041$ K: Curie temperature of iron, $T_{RT} = 300$ K: room temperature, fluence $F = 10$ mJ/cm^2). (c) Orientation probability of the in-plane magnetization shown in (g) and (h), demonstrating the transition from an oriented magnetic ripple structure into a largely isotropic vortex network. (d)–(f) Electron micrographs with Lorentz contrast before (e) and after (d),(f) applying a single femtosecond laser pulse (optical fluence $F = 12.7$ mJ/cm^2). [The dark blue regions in the corners of (d) correspond to the opaque silicon support frame.] (g),(h) Reconstructed in-plane magnetization for the Lorentz images shown in (e) and (f), respectively. Color saturation and hue signify the normalized magnitude and direction of the local magnetization [see color wheel in (g)]. Close-ups of the marked areas in (f) and (h) are shown in Fig. 2. [Equal length scales are chosen in (e)–(h). Electron intensity and magnetization were normalized to the maximum values in (f) and (h), respectively.]

substrate. The estimated temperature transients of both layers in the center of the laser profile are shown in Fig. 1(b) for a peak optical fluence of $F = 10$ mJ/cm^2 (see Supplemental Material [33] for details) [50]. Notably, in this configuration, cooling rates larger than 10^{12} K/s are achieved in the iron layer.

Figures 1(e) and 1(f) display Lorentz electron micrographs of the magnetic bilayer before and after applying a single femtosecond laser pulse, respectively (see also Supplemental Material [33], Movie S1). For an optical excitation above a well-defined fluence threshold of $F = 11.5$ mJ/cm^2, the initial magnetic structure within a sharply demarcated area at the center of the optical focus undergoes a remarkable change [Fig. 1(d)], from a weak meanderlike contrast [Fig. 1(e)] to an image with high-contrast hot and cold spots [Fig. 1(f)]. Optical pulses below this threshold only result in increased domain wall mobility with no large-scale magnetic reorganization (see Supplemental Material [33] and Movie S2).

From the Lorentz micrographs, we reconstruct the underlying in-plane magnetization for both cases [Figs. 1(g) and 1(h)], using a transport-of-intensity approach [32,51] (see Supplemental Material [33]). Prior to optical excitation, the magnetic texture in the iron thin film shows a ripple structure [52] with two preferred antiparallel magnetization directions [cf. Fig. 1(c), blue curve]. After optical excitation, the magnetic structure exhibits no preferred orientation [Fig. 1(c), red curve] but instead is characterized by a large number of nanoscale domains.

Figures 2(a) and 2(c) display the Lorentz micrograph and the reconstructed in-plane magnetization of a small sample area [marked in Figs. 1(f) and 1(h)], respectively. Vortices and antivortices are formed at domain junctions, yielding a dense defect network. At each magnetic vortex [open (dotted) white discs], the in-plane magnetization curls in a clockwise (counterclockwise) direction around a central point leading to a local focusing (defocusing) of the incident electron beam due to the Lorentz force. Thereby, bright (dark) contrasts are generated in the Lorentz images [53]. Between vortices with equal curling direction, antivortices are located (red circles), which are discernible as saddle points in image intensity.

In Fig. 2(b), the spatial distribution of topological defect types within the network is rationalized by considering the local phase imprinted on the transmitted electron microscope beam. Here, clockwise and counterclockwise vortices correspond to maxima and minima in the phase map, respectively, whereas antivortices can be seen as saddle points. A path from one phase basin to the next can be naturally chosen to include a saddle point, resulting in an interwoven network with alternating vortex and antivortex nodes [Fig. 2(d)].

A more detailed analysis of the average distances between these defects is obtained from radial pair-correlation functions [cf. Fig. 3(d) at $F = 14.4$ mJ/cm^2], involving equally rotating vortices (ϱ_{vv}, green curve), vortices and antivortices (ϱ_{av}, red curve), and vortices with different

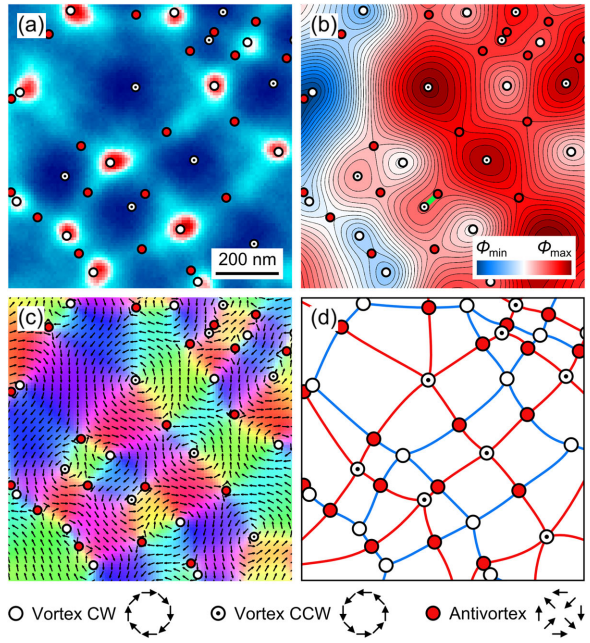

FIG. 2. Magnetic network structure. (a),(c) Lorentz micrograph (a) and corresponding reconstructed in-plane magnetization (c) for the sample area indicated in Figs. 1(f) and 1(h). The positions of clockwise (CW) and counterclockwise (CCW) rotating vortices and antivortices were retrieved from the magnetization maps and are indicated as white and red circles, respectively [color scales equal to Figs. 1(f) and 1(h), respectively; vectors in (c) indicate magnetization direction]. (b) Reconstructed local phase which is imprinted by the magnetic network onto the imaging electron wave. Phase minima (maxima) result in an electron beam focusing (defocusing) leading to image intensity maxima (minima). Antivortices are located at saddle points of the phase surface. The green bar indicates a close-by vortex-antivortex pair. (d) Topology of the vortex-antivortex network constructed from the phase map in (b) following the steepest ascent and descent paths, which start at each phase saddle point.

rotation directions (ϱ_{vv^*}, blue curve). ϱ_{av} and ϱ_{vv^*} exhibit pronounced maxima (at 80 and 150 nm, respectively), demonstrating short-range order between neighboring nodes in the defect network. ϱ_{vv} displays only a very weak maximum around 200 nm. In addition, we find a minimal node distance of 50–100 nm, leading to an excluded area around each defect. We note that the magnetic configuration arising from a pair of close-by vortex and antivortex defects can be locally transformed into a defect-free state [54], resulting in hairpin-like equal-phase curves as indicated in Fig. 2(b) for one connected vortex-antivortex pair (green bar). Similar to atomic pair-correlation functions of glasses and liquids, no spatial network ordering is observed beyond nearest neighbor distances. Furthermore, for subsequent above-threshold laser pulses, the position of vortices and antivortices on the sample is randomly distributed within the center of the excited sample region (Supplemental Material [33], Fig. S5), highlighting that pinning sites [4] on length scales larger than the grain size of the polycrystalline iron film only play a minor role.

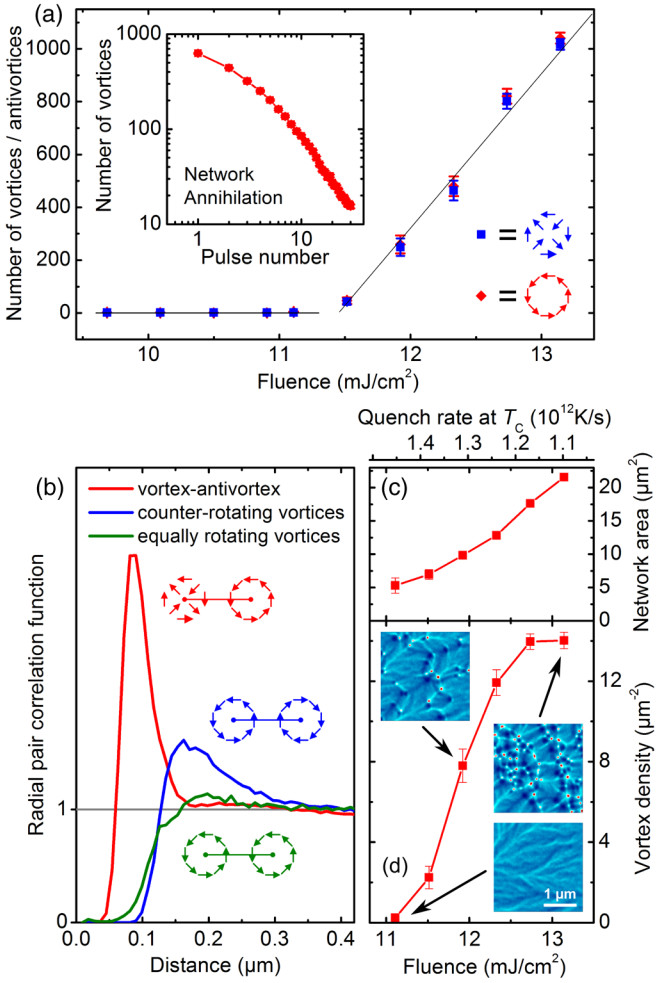

FIG. 3. Fluence dependencies and spatial network dimensions. (a) Experimentally observed total number of vortices and antivortices after applying single laser pulses with a varying optical fluence F, exhibiting a well-defined fluence threshold of about 11.5 mJ/cm^2. Inset: Optically triggered defect annihilation below fluence threshold. Starting with a vortex-antivortex network generated above threshold, subsequent optical pulses at $F = 10.8$ mJ/cm^2 restore the magnetic ripple structure. (b) Experimental radial pair-correlation function between the position of vortices and antivortices (ϱ_{av}, red), and equal- (ϱ_{vv}, green) and counterrotating (ϱ_{vv^*}, blue) vortices. (c) Fluence-dependent area of the vortex-antivortex network ($A = \pi\sigma_x\sigma_y$), defined by the standard deviations $\sigma_{x,y}$ of vortex positions in both spatial directions. (d) Vortex density depending on the excitation fluence, reaching a maximum value of about 14 vortices/μm^2. The insets show representative electron micrographs at the indicated fluences. The estimated quench rate at T_C is shown for the employed fluence range.

In Fig. 3(a), the number of laser-generated vortices and antivortices is displayed for different optical fluences, observing a linear increase above a well-defined fluence threshold. Taking into account the fluence-dependent network area yields a saturation behavior of the defect density at high fluences [cf. Figs. 3(e) and 3(f)]. Vortices and antivortices are

topological defects which can be characterized by a winding number $w = 1/2\pi \oint \nabla\alpha \cdot ds$ yielding $w = \pm 1$ for vortices and antivortices, respectively (α: local orientation of in-plane magnetization vector) [54]. The integral extends over an arbitrary contour containing the magnetic singularities, so that locally confined magnetization changes conserve the total winding number in the affected area. Consequentially, as observed here, an equal number of laser-generated vortices and antivortices is expected after optical excitation.

The spontaneous generation of vortices and antivortices by light in a homogeneous magnetic thin film may at first seem surprising. In localized nanoparticles, vortex structures are typically found as the lowest-energy configuration, stabilized by stray field minimization [2–5,55], whereas for homogeneous thin films, as studied here, vortex structures are excited states. Nevertheless, we find the laser-induced vortex-antivortex network to be stable at room temperature, and no relaxation to the equilibrium magnetic ripple structure is observed over a time span of several months. However, in a creeplike process, vortex-antivortex annihilation processes can be facilitated by applying optical pulses with a fluence slightly below the threshold for vortex-antivortex generation. The decrease of the number of vortices for subsequent intermediate intensity pulses is quantified in the inset of Fig. 3(a), with the equilibrium magnetic ripple pattern completely regained after several tens of optical pulses (see Supplemental Material [33], Movie S3, for a sequence of Lorentz images). The lack of long-range order and the appearance of creep are indicative of a glasslike state, which differentiates the light-induced magnetic vortex-antivortex network from a supercooled high-temperature equilibrium magnetic phase [56], and points to similarities to the behavior of structural glasses as well as phase-change materials [57,58].

In the following, we describe in more detail the generation mechanism leading to the formation of the vortex-antivortex network. After optical excitation, the magnetic structure of the iron film will be strongly altered when its peak spin temperature exceeds the Curie temperature. At the ferromagnetic phase transition, the averaged local magnetization approaches zero, leading to a substantial decrease in the magnetic dipolar couplings and a vanishing magnetic shape anisotropy energy, and to a divergent magnetic response time upon external perturbations [59]. Slowed-down dynamics at second-order phase transitions were invoked first by Kibble [23] in a cosmological context and later for condensed matter systems by Zurek [24] to predict the appearance of topologically protected configurations when crossing the phase transition at finite cooling rates. In particular, critical fluctuations of the high temperature phase freeze out close to the phase transition, so that features of the high temperature phase are introduced into the newly formed symmetry-broken phase as topological defect states. In agreement with a KZM-like picture, we observe vortex-antivortex generation for optical fluences exceeding $F = 11.5$ mJ/cm^2 [cf. Fig. 3(a), for which the peak temperature is estimated to be above the Curie temperature (estimated peak temperature at threshold: ~1400 K). However, we note that the relation between the dimensionality and length scales of the relevant critical fluctuations and the characteristics of the observed vortex-antivortex network remains an open question.

The average node distance within the vortex-antivortex network of about 100 nm [Fig. 3(d)] reflects the correlation length l_c of the newly formed magnetic texture, and, within the KZM, is expected to be given by the length scale of the relevant critical fluctuations, which decreases with an increasing quench rate [24]. Such a behavior was, e.g., found in the case of a ferroelectric phase transition for quench rates in the range of 10–10^4 K/h [25]. The ultrafast quenching scheme employed here with cooling rates larger than 10^{12} K/s is not readily adaptable to larger changes in the quench rate. Specifically, we estimate that cooling rates at the phase transition temperature vary by only a factor of 1.3 in the investigated fluence interval, with the highest quench rates close to the threshold fluence. Contrary to the predictions of the KZM, the largest vortex density is experimentally observed at the highest fluence values, i.e., at the smallest quench rates at T_C [Fig. 3(f)]. Such a scaling may be caused by vortex-antivortex annihilation events occurring after the phase transition, or by boundary effects between the vortex-antivortex network and the surrounding ripple domain area.

Many aspects of the experimentally observed vortex-antivortex generation, including the threshold behavior, vortex-antivortex annihilation, and the appearance of defect networks with fluidlike pair-correlation functions, can be qualitatively described by the quench behavior of a simplified classical two-dimensional XY model (see Supplemental Material [33]) [54]. In this model, spin orientation is limited to in-plane orientation, and only short-range ferromagnetic exchange is considered. However, the iron thin film exhibits a quasi-2D character of the magnetization only in the low-temperature ferromagnetic phase (induced by dipolar interactions) [60], whereas in the high-temperature paramagnetic state orientational spin confinement is relaxed. Thereby, in the paramagnetic state, vortices and antivortices lose their topologically protected character. The quench-induced generation of topological defects therefore involves both a local alignment of spins upon cooling below the Curie temperature, and a buildup of the film's magnetic shape anisotropy, induced by medium-range magnetic dipole interactions within individual domains. A more quantitative description of the magnetic quench process would require computationally demanding, time-dependent 3D-micromagnetic simulations covering both the atomistic length scales of the fluctuations in the paramagnetic phase, potentially in a coarse-grained manner, and the 100 nm length scales of the vortex-antivortex network. Further theoretical investigations are needed to disentangle the spatiotemporal coupling of the emerging local magnetization anisotropy and the occurrence of topological defects. Specifically, it will be important

to elucidate the nature of critical fluctuations at the phase transition and their influence on the resulting defect states.

Finally, we note that the excitation and quenching conditions necessary to induce a nanoscale vortex-antivortex network are similar to the ones typically employed in helicity-dependent all-optical switching [61,62], and metastable states, as observed here, may generally play an important role in the manipulation of magnetic structures by intense light.

In conclusion, we demonstrated the optically triggered formation of a magnetic vortex-antivortex texture and analyzed its structural properties using *in situ* Lorentz microscopy. Rapid quenching preserves a high density of topological defects, which arranges in an extended network structure. This approach may give access to a host of metastable configurations in various magnetic materials, and provides novel opportunities to unravel nanoscale ordering mechanisms far from equilibrium, complementary to emerging approaches in ultrafast transmission electron microscopy [63,64].

We gratefully acknowledge fruitful discussions with K. Samwer and M. Plenio. Financial support was provided by the Deutsche Forschungsgemeinschaft (DFG-SFB 1073/ Projects No. A05 and No. B01), the VolkswagenStiftung, and the Lower Saxony Ministry of Science and Culture. M. M. and N. R. acknowledge a scholarship by the Studienstiftung des deutschen Volkes e.V. and CNPq, Brazil, respectively.

T. E. and M. M. contributed equally to this work.

*schaefer@ph4.physik.uni-goettingen.de

[1] H.-B. Braun, Topological effects in nanomagnetism: from superparamagnetism to chiral quantum solitons, Adv. Phys. **61**, 1 (2012).

[2] T. Shinjo, T. Okuno, R. Hassdorf, K. Shigeto, and T. Ono, Magnetic vortex core observation in circular dots of permalloy, Science **289**, 930 (2000).

[3] A. Wachowiak, J. Wiebe, M. Bode, O. Pietzsch, M. Morgenstern, and R. Wiesendanger, Direct observation of internal spin structure of magnetic vortex cores, Science **298**, 577 (2002).

[4] T. Uhlig, M. Rahm, C. Dietrich, R. Höllinger, M. Heumann, D. Weiss, and J. Zweck, Shifting and Pinning of a Magnetic Vortex Core in a Permalloy Dot by a Magnetic Field, Phys. Rev. Lett. **95**, 237205 (2005).

[5] P. Szary, O. Petracic, F. Brüssing, M. Ewerlin, and H. Zabel, Indication of vortex stabilization and buckling in circular shaped magnetic nanostructures, J. Appl. Phys. **107**, 113922 (2010).

[6] S. D. Pollard, L. Huang, K. S. Buchanan, D. A. Arena, and Y. Zhu, Direct dynamic imaging of non-adiabatic spin torque effects, Nat. Commun. **3**, 1028 (2012).

[7] U. K. Rößler, A. N. Bogdanov, and C. Pfleiderer, Spontaneous skyrmion ground states in magnetic metals, Nature (London) **442**, 797 (2006).

[8] N. Nagaosa and Y. Tokura, Topological properties and dynamics of magnetic skyrmions, Nat. Nanotechnol. **8**, 899 (2013).

[9] S. Mühlbauer, B. Binz, F. Jonietz, C. Pfleiderer, A. Rosch, A. Neubauer, R. Georgii, and P. Böni, Skyrmion lattice in a chiral magnet, Science **323**, 915 (2009).

[10] X. Z. Yu, Y. Onose, N. Kanazawa, J. H. Park, J. H. Han, Y. Matsui, N. Nagaosa, and Y. Tokura, Real-space observation of a two-dimensional skyrmion crystal, Nature (London) **465**, 901 (2010).

[11] S. Heinze, K. von Bergmann, M. Menzel, J. Brede, A. Kubetzka, R. Wiesendanger, G. Bihlmayer, and S. Blügel, Spontaneous atomic-scale magnetic skyrmion lattice in two dimensions, Nat. Phys. **7**, 713 (2011).

[12] M. Kläui, C. A. F. Vaz, J. A. C. Bland, W. Wernsdorfer, G. Faini, E. Cambril, L. J. Heyderman, F. Nolting, and U. Rüdiger, Controlled and Reproducible Domain Wall Displacement by Current Pulses Injected into Ferromagnetic Ring Structures, Phys. Rev. Lett. **94**, 106601 (2005).

[13] K. Yamada, S. Kasai, Y. Nakatani, K. Kobayashi, H. Kohno, A. Thiaville, and T. Ono, Electrical switching of the vortex core in a magnetic disk, Nat. Mater. **6**, 270 (2007).

[14] W. Jiang, P. Upadhyaya, W. Zhang, G. Yu, M. B. Jungfleisch, F. Y. Fradin, J. E. Pearson, Y. Tserkovnyak, K. L. Wang, O. Heinonen, S. G. E. te Velthuis, and A. Hoffmann, Blowing magnetic skyrmion bubbles, Science **349**, 283 (2015).

[15] B. Van Waeyenberge, A. Puzic, H. Stoll, K. W. Chou, T. Tyliszczak, R. Hertel, M. Fähnle, H. Brückl, K. Rott, G. Reiss, I. Neudecker, D. Weiss, C. H. Back, and G. Schütz, Magnetic vortex core reversal by excitation with short bursts of an alternating field, Nature (London) **444**, 461 (2006).

[16] F. Büttner, C. Moutafis, M. Schneider, B. Krüger, C. M. Günther, J. Geilhufe, C. v. K. Schmising, J. Mohanty, B. Pfau, S. Schaffert, A. Bisig, M. Foerster, T. Schulz, C. A. F. Vaz, J. H. Franken, H. J. M. Swagten, M. Kläui, and S. Eisebitt, Dynamics and inertia of skyrmionic spin structures, Nat. Phys. **11**, 225 (2015).

[17] G. E. W. Bauer, E. Saitoh, and B. J. van Wees, Spin caloritronics, Nat. Mater. **11**, 391 (2012).

[18] F. Schlickeiser, U. Ritzmann, D. Hinzke, and U. Nowak, Role of entropy in domain wall motion in thermal gradients, Phys. Rev. Lett. **113**, 097201 (2014).

[19] M. Finazzi, M. Savoini, A. R. Khorsand, A. Tsukamoto, A. Itoh, L. Duò, A. Kirilyuk, T. Rasing, and M. Ezawa, Laser-induced magnetic nanostructures with tunable topological properties, Phys. Rev. Lett. **110**, 177205 (2013).

[20] R. Hertel and C. M. Schneider, Exchange explosions: Magnetization dynamics during vortex-antivortex annihilation, Phys. Rev. Lett. **97**, 177202 (2006).

[21] R. D. Gomez, J. S. Ma, A. Arkilic, S. H. Chung, and C. Krafft, Vortex-antivortex creation and annihilation on CoFeB crosstie patterns, J. Appl. Phys. **109**, 07D310 (2011).

[22] M. Kammerer, M. Weigand, M. Curcic, M. Noske, M. Sproll, A. Vansteenkiste, B. Van Waeyenberge, H. Stoll, G. Woltersdorf, C. H. Back, and G. Schuetz, Magnetic vortex core reversal by excitation of spin waves, Nat. Commun. **2**, 279 (2011).

[23] T. W. B. Kibble, Topology of cosmic domains and strings, J. Phys. A **9**, 1387 (1976).
[24] W. H. Zurek, Cosmological experiments in superfluid helium?, Nature (London) **317**, 505 (1985).
[25] S.-Z. Lin, X. Wang, Y. Kamiya, G.-W. Chern, F. Fan, D. Fan, B. Casas, Y. Liu, V. Kiryukhin, W. H. Zurek, C. D. Batista, and S.-W. Cheong, Topological defects as relics of emergent continuous symmetry and Higgs condensation of disorder in ferroelectrics, Nat. Phys. **10**, 970 (2014).
[26] I. Chuang, R. Durrer, N. Turok, and B. Yurke, Cosmology in the laboratory: Defect dynamics in liquid crystals, Science **251**, 1336 (1991).
[27] S. Deutschländer, P. Dillmann, G. Maret, and P. Keim, Kibble-Zurek mechanism in colloidal monolayers, Proc. Natl. Acad. Sci. U.S.A. **112**, 6925 (2015).
[28] S. M. Griffin, M. Lilienblum, K. T. Delaney, Y. Kumagai, M. Fiebig, and N. A. Spaldin, Scaling behavior and beyond equilibrium in the hexagonal manganites, Phys. Rev. X **2**, 041022 (2012).
[29] V. M. H. Ruutu, V. B. Eltsov, A. J. Gill, T. W. B. Kibble, M. Krusius, Y. G. Makhlin, B. Placais, G. E. Volovik, and W. Xu, Vortex formation in neutron-irradiated superfluid ^{3}He as an analogue of cosmological defect formation, Nature (London) **382**, 334 (1996).
[30] C. Bäuerle, Y. M. Bunkov, S. N. Fisher, H. Godfrin, and G. R. Pickett, Laboratory simulation of cosmic string formation in the early universe using superfluid ^{3}He, Nature (London) **382**, 332 (1996).
[31] S. Ulm, J. Roßnagel, G. Jacob, C. Degünther, S. T. Dawkins, U. G. Poschinger, R. Nigmatullin, A. Retzker, M. B. Plenio, F. Schmidt-Kaler, and K. Singer, Observation of the Kibble-Zurek scaling law for defect formation in ion crystals, Nat. Commun. **4**, 2290 (2013).
[32] A. K. Petford-Long and M. De Graef, Lorentz Microscopy, in *Characterization of Materials* (John Wiley & Sons, Inc., New York, 2002).
[33] See Supplemental Material at http://link.aps.org/supplemental/10.1103/PhysRevLett.118.097203, which includes Refs. [34–49], for further details, regarding the thermal transient after optical excitation, Lorentz microscopy and the reconstruction of sample magnetization, processes occurring below the excitation threshold for vortex generation, and the simulation of a quenched vortex state within a simple two-dimensional XY model.
[34] E. Beaurepaire, J.-C. Merle, A. Daunois, and J.-Y. Bigot, Ultrafast Spin Dynamics in Ferromagnetic Nickel, Phys. Rev. Lett. **76**, 4250 (1996).
[35] E. Carpene, E. Mancini, C. Dallera, M. Brenna, E. Puppin, and S. De Silvestri, Dynamics of electron-magnon interaction and ultrafast demagnetization in thin iron films, Phys. Rev. B **78**, 174422 (2008).
[36] T. Kampfrath, R. G.Ulbrich, F. Leuenberger, M. Münzenberg, B. Sass, and W. Felsch, Ultrafast magneto-optical response of iron thin films, Phys. Rev. B **65**, 104429 (2002).
[37] J. Mendil, P. Nieves, O. Chubykalo-Fesenko, J. Walowski, T. Santos, S. Pisana, and M. Münzenberg, Resolving the role of femtosecond heated electrons in ultrafast spin dynamics, Sci. Rep. **4**, 3980 (2014).
[38] T. Jeong, J.-G. Zhu, S. Chung, and M. R. Gibbons, Thermal boundary resistance for gold and CoFe alloy on silicon nitride films, J. Appl. Phys. **111**, 083510 (2012).
[39] W. Liang, S. Schäfer, and A. H. Zewail, Ultrafast electron crystallography of heterogeneous structures: Gold-graphene bilayer and ligand-encapsulated nanogold on graphene, Chem. Phys. Lett. **542**, 8 (2012).
[40] A. Kohn and A. Habibi, Adapting a JEM-2100F for magnetic imaging by Lorentz TEM, JEOL News **47**, 17 (2012).
[41] J. Lau, M. Schofield, and Y. Zhu, A straightforward specimen holder modification for remnant magnetic-field measurement in TEM, Ultramicroscopy **107**, 396 (2007).
[42] *Magnetic Imaging and Its Applications to Materials*, edited by M. De Graef and Y. Zhu (Academic Press, San Diego, 2000).
[43] E. Humphrey, C. Phatak, A. Petford-Long, and M. De Graef, Separation of electrostatic and magnetic phase shifts using a modified transport-of-intensity equation, Ultramicroscopy **139**, 5 (2014).
[44] J. M. Kosterlitz and D. J. Thouless, Ordering, metastability and phase transitions in two-dimensional systems, J. Phys. C **6**, 1181 (1973).
[45] V. Berezinskii, Destruction of long-range order in one-dimensional and two-dimensional systems having a continuous symmetry group I. Classical systems, Sov. Phys. JETP **32**, 493 (1971).
[46] L. Berthier, P. C. W. Holdsworth, and M. Sellitto, Nonequilibrium critical dynamics of the two-dimensional XY model, J. Phys. A **34**, 1805 (2001).
[47] A. Jelić and L. F. Cugliandolo, Quench dynamics of the 2d XY model, J. Stat. Mech. (2011) P02032.
[48] N. Metropolis, A. W. Rosenbluth, M. N. Rosenbluth, A. H. Teller, and E. Teller, Equation of state calculations by fast computing machines, J. Chem. Phys. **21**, 1087 (1953).
[49] G. Biroli, L. F. Cugliandolo, and A. Sicilia, Kibble-Zurek mechanism and infinitely slow annealing through critical points, Phys. Rev. E **81**, 050101 (2010).
[50] For the time scales considered here, electron, lattice, and spin subsystems are expected to be in local equilibrium, which is described by a common temperature T.
[51] V. Volkov, Y. Zhu, and M. De Graef, A new symmetrized solution for phase retrieval using the transport of intensity equation, Micron **33**, 411 (2002).
[52] S. Methfessel, S. Middelhoek, and H. Thomas, Partial rotation in permalloy films, J. Appl. Phys. **32**, 1959 (1961).
[53] M. De Graef, *Introduction to Conventional Transmission Electron Microscopy* (Cambridge University Press, Cambridge, 2003).
[54] P. M. Chaikin and T. C. Lubensky, *Principles of Condensed Matter Physics* (Cambridge University Press, Cambridge, 2000).
[55] K. Shigeto, T. Okuno, K. Mibu, T. Shinjo, and T. Ono, Magnetic force microscopy observation of antivortex core with perpendicular magnetization in patterned thin film of permalloy, Appl. Phys. Lett. **80**, 4190 (2002).
[56] H. Oike, A. Kikkawa, N. Kanazawa, Y. Taguchi, M. Kawasaki, Y. Tokura, and F. Kagawa, Interplay between topological and thermodynamic stability in a metastable magnetic skyrmion lattice, Nat. Phys. **12**, 62 (2016).

[57] M. Wuttig and N. Yamada, Phase-change materials for rewriteable data storage, Nat. Mater. **6**, 824 (2007).
[58] T. Tuma, A. Pantazi, M. Le Gallo, A. Sebastian, and E. Eleftheriou, Stochastic phase-change neurons, Nat. Nanotechnol. **11**, 693 (2016).
[59] O. Chubykalo-Fesenko, U. Nowak, R. W. Chantrell, and D. Garanin, Dynamic approach for micromagnetics close to the Curie temperature, Phys. Rev. B **74**, 094436 (2006).
[60] A. Hubert and R. Schäfer, *Magnetic Domains: The Analysis of Magnetic Microstructures* (Springer, Berlin, 2008).
[61] C. D. Stanciu, F. Hansteen, A. V. Kimel, A. Kirilyuk, A. Tsukamoto, A. Itoh, and T. Rasing, All-optical magnetic recording with circularly polarized light, Phys. Rev. Lett. **99**, 047601 (2007).
[62] C.-H. Lambert, S. Mangin, B. S. D. C. S. Varaprasad, Y. K. Takahashi, M. Hehn, M. Cinchetti, G. Malinowski, K. Hono, Y. Fainman, M. Aeschlimann, and E. E. Fullerton, All-optical control of ferromagnetic thin films and nanostructures, Science **345**, 1337 (2014).
[63] A. H. Zewail, Four-dimensional electron microscopy, Science **328**, 187 (2010).
[64] A. Feist, K. E. Echternkamp, J. Schauss, S. V. Yalunin, S. Schäfer, and C. Ropers, Quantum coherent optical phase modulation in an ultrafast transmission electron microscope, Nature (London) **521**, 200 (2015).